Journal of Fluids and Structures (2002) **16**(2), 193–212
doi:10.1006/jfls.2001.0415, available online at http://www.idealibrary.com on IDEAL®

DYNAMICS OF MOORING CABLES IN RANDOM SEAS

A. Sarkar and R. E. Taylor

Department of Engineering Science, University of Oxford, Parks Road Oxford OX1 3PJ, U.K.

(Received 11 February 1999, and in final form 10 May 2001)

The dynamic analysis of a catenary mooring cable due to random motion of an offshore platform is performed in the frequency domain. The nonlinear fluid-drag force is linearized using the statistical linearization technique. A previously developed numerical procedure based on converting a boundary value problem to an equivalent set of initial value problems is utilized to solve the problem, which avoids the need for modal analysis. The method is found to be versatile for the determination of spatially varying drag and the analysis of composite cables in a unified manner. The influence of current on drag damping has also been investigated. The effect of seabed friction damping has also been incorporated in the linearized analysis.

1. INTRODUCTION

Mooring cables are typically used to maintain a floating offshore platform in position in a multidirectional wave and wind environment. Recently, it has been pointed out that the dynamic behaviour of the mooring itself can be important in calculating the response of the floating platform (Nakamura *et al.* 1991). Moreover, the hydrodynamic drag in moorings can be a major source of damping (up to 80% of total damping), which can significantly reduce the vessel response and dynamic cable tension (Huse & Matsumoto 1989). The main difficulty in solving the problem is that no closed-form solution is available for the dynamic equations of motion of a cable; in addition, the presence of quadratic hydrodynamic drag complicates the analysis further. Typically, the total damping on a floating offshore structure is very low. As the dynamic response amplitude is sensitive to damping, it is therefore necessary to make an accurate determination of the damping on the mooring system, including that due to drag. The nonlinear drag is conventionally linearized by the statistical linearization technique, so that approximate frequency-domain analysis can be performed using the finite-element technique. As the system is nonproportionally damped, a complex eigenvalue analysis becomes essential. Moreover, it is necessary to take a large number of elements in the computation to obtain the linearized drag damping accurately along the length of a mooring cable. Accordingly, the problem size increases significantly for the coupled analysis of cable and vessel assembly. Sometimes, a significant portion of the cable lies on the ocean floor, which alternately lifts off and drops back under dynamic conditions. This effect gives rise to additional complexity, as it makes the system model time-dependent. The interaction between seabed and cable also gives rise to frictional forces which may influence the dynamic response of the cable.

Extensive research has been carried out in the past concerning the dynamics of marine cables. Some of the important studies are the following. Finite-element representations have been developed by Peyrot (1980) and Leonard & Tuah (1989). Different time-domain

0889–9746/02/020193 + 20 $35.00/0

schemes have been applied by Nakamura *et al.* (1991) and Huang (1994) to solve the dynamic equations of the marine cable. Triantafyllou *et al.* (1985) carried out, in the linear cable dynamics, the identification of interesting phenomena such as modal crossover of symmetric and antisymmetric modes and then described the effects of nonlinear fluid drag, geometric nonlinearity and cable–seabed interactions. Originally developed by Bliek (1984), Hover *et al.* (1994) used a transfer matrix approach (based on a finite-difference scheme) in the frequency domain using equivalent linearization of the hydrodynamic drag. Webster (1995) carried out extensive parametric investigations of the cable dynamic behaviour due to harmonic support motions, using a nonlinear finite-element technique. The important influence of mooring line damping on the response of the vessel has been highlighted by Huse & Matsumoto (1989), based on some experimental results. Some details of more recent investigations of mooring line drag damping have been given by Brown *et al.* (1995). Thomas & Hearn (1994) developed a time-domain finite-difference scheme, using a lumped mass approach to account for both the seabed friction effects as well as the lifting and grounding of the seabed-lying portion of the cable. The approximate treatment of the seabed friction in the frequency domain has been outlined by Liu & Bergdahl (1997a, b), ignoring the lifting-off effect. Liu & Bergdahl (1997b) also compared results from frequency- and time-domain simulations. Recently, Kitney & Brown (1998) developed a time-domain simulation technique with experimental verification to determine the drag damping due to harmonic and biharmonic support oscillation of the top end of the cable, based on a quasistatic approach which assumes that the cable maintains its catenary profile at all times.

The present work is carried out in order to study the effect of mooring-induced damping on the extreme responses of a floating body. In many circumstances, the response of a moored floating body is dominated by large-amplitude slow-drift resonant response to second-order wave-induced hydrodynamic forces. The second-order force and response are nonGaussian in a Gaussian random sea. The damping of such a system is generally small and, as pointed out by Huse & Matsumoto (1989), the mooring line damping can constitute a major portion of the total damping. It therefore requires accurate estimating, since the system is very sensitive to damping. The wave frequency first-order wave-induced responses can significantly influence the mooring line drag damping, and through this the slow drift response.

Using a nonlinear spectral analysis technique based on a Volterra series model, in conjunction with the Kac–Seigert method, a probabilistic analysis was undertaken by Sarkar & Eatock Taylor (2000). This led to a study of the influence of spatially varying mooring line drag damping on the nonGaussian response of a floating body moored by taut catenaries. The aim of the present investigation was to avoid the need for time-domain integration in evaluating random wave-induced responses, while retaining in a frequency-domain analysis the influence of the spatially varying fluid drag. We have extended the approach developed by Sarkar & Manohar (1996) for obtaining the dynamic stiffness matrix of a general cable element, in order to analyse the in-plane behaviour of a mooring cable. The quadratic drag force has been linearized by using the method of stochastic linearization. The motions of the floating platform have been modelled as stationary Gaussian vector random processes, which act as support excitations of the mooring cable. The determination of linearized damping, which is an unknown function along the length of the cable, requires the solution of an associated quasistatic boundary value problem. Unfortunately, no closed-form solution exists for these equations. In the present approach, the boundary value problem has been converted into an equivalent set of initial value problems, as described in Sections 2 and 3. These are solved directly, using numerical integration techniques. A distinguishing feature of this approach is that it avoids the need

for carrying out a complex eigenvalue analysis which, for modal expansion methods, is an inevitable first step. It can also elegantly handle the varying material and geometric properties of a cable, such as in the case of a composite mooring system made of different segments. When a significant length of a mooring cable lies on the ocean floor, the damping arising from the interaction of the mooring cable and the seabed due to out-of-plane motion has also been determined in the linearized analysis. This is summarized in Section 4. Numerical results are presented in Section 5 showing the effect of different parameters on the mooring line responses.

The emphasis of this work is on illustrating how the influence of local amplitude-dependent drag damping can be accounted for when the cable is excited stochastically. As far as we are aware, this has not previously been investigated in this way, and there are no results in the literature with which ours may be directly compared. In particular, the work of Triantafyllou *et al.* (1985), while bearing some similarity to the present work, does not deal with the aspect of spatially varying drag damping induced by random excitation. We have therefore attempted to validate our results by checking a number of standard results. This is described in Section 5.

2. EQUATIONS OF IN-PLANE MOTION

We use a Cartesian coordinate system Oxy located at the bottom end of the cable, with Ox pointing along the chord of the mean configuration and Oy pointing down, as shown in Figure 1. The motions of the right-hand end of the cable are specified as X and Y. Considering the equilibrium of an infinitesimal element of the cable shown in Figure 1, we can write the equations governing the static profile and corresponding tension $T_s(s)$ as

$$\frac{\mathrm{d}}{\mathrm{d}s}\left[\left(\frac{T_s(s)}{1 + T_s(s)/EA}\right)\frac{\mathrm{d}x}{\mathrm{d}s}\right] = m_s g \sin\theta, \tag{1}$$

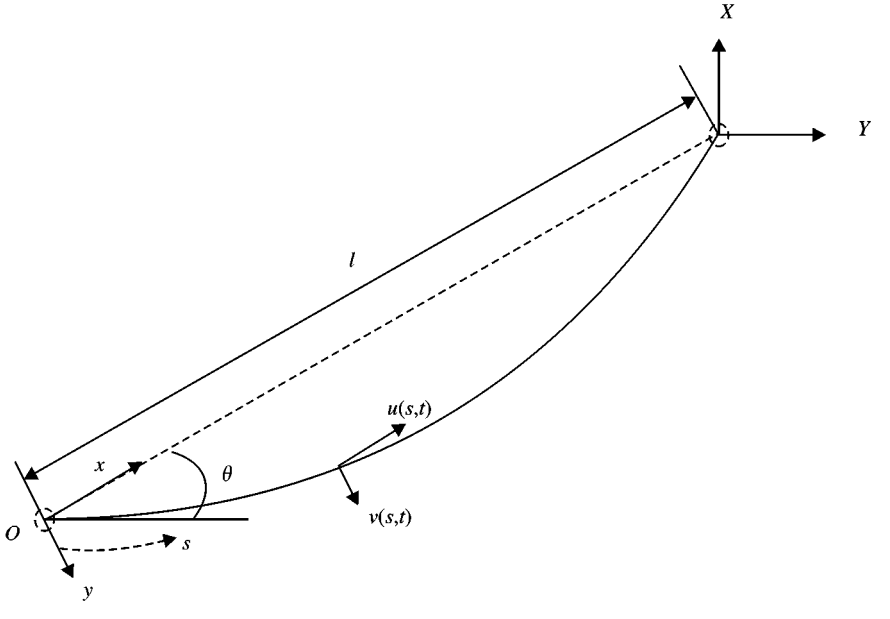

Figure 1. Schematic diagram of a mooring cable.

$$\frac{\mathrm{d}}{\mathrm{d}s}\left[\left(\frac{T_s(s)}{1+T_s(s)/EA}\right)\frac{\mathrm{d}y}{\mathrm{d}s}\right] = -m_s g\cos\theta, \tag{2}$$

$$\left(\frac{\mathrm{d}x}{\mathrm{d}s}\right)^2 + \left(\frac{\mathrm{d}y}{\mathrm{d}s}\right)^2 = \left(1+\frac{T_s(s)}{EA}\right)^2, \tag{3}$$

where s is the arc length of the cable in the unstretched state, EA is the axial stiffness of the cable, m_s is the mass per unit length in water, θ is the inclination of the cable chord with the horizontal and g is the acceleration due to gravity. These equations are similar to those given by Hagedorn & Schäfer (1980) for a horizontal cable, but modified to account for the inclination of the chord.

From equations (1)–(3), the following relationships can be obtained:

$$\frac{\mathrm{d}x}{\mathrm{d}s} = \frac{H(s)}{T_s(s)}\left(1+\frac{T_s(s)}{EA}\right), \tag{4}$$

$$\frac{\mathrm{d}y}{\mathrm{d}s} = \frac{m_s g\cos\theta(L/2-s)}{T_s(s)}\left(1+\frac{T_s(s)}{EA}\right), \tag{5}$$

$$T_s^2(s) = H(s)^2 + (m_s g\cos\theta)^2(L/2-s)^2, \tag{6}$$

$$H(s) = H_0 + \frac{m_s g L}{2}\sin\theta[(2s/L)-1], \tag{7}$$

where L is the length of the unstretched cable, $H(s)$ is the axial component of the cable tension (i.e., in the direction of Ox) with the value H_0 at the midspan ($s = L/2$). The semianalytical solutions of equations (1)–(3) for the equilibrium positions $x(s)$ and $y(s)$ are given by Irvine (1981) (although in a different coordinate system). However, equations (4)–(7) are sufficient for the linear dynamic analysis as discussed subsequently.

By considering an infinitesimal cable element, we can define the equations governing the total dynamic displacements $u_t(s,t)$ and $v_t(s,t)$ along the directions of the x- and y-axis, respectively, following Simpson (1972) and Hagedorn & Schäfer (1980). The mooring cable is assumed to have the following parameters: m is the mass per unit length of the cable (including added mass); ρ_w is the density of water; d is the diameter of the cable; $C_n^d = \frac{1}{2}\rho_w C_d d$; C_d is the coefficient of cable normal drag; C_v^s and C_u^s are structural damping coefficients; and V_x and V_y are the components of the current velocity along the cable in the direction of $u_t(s,t)$ and $v_t(s,t)$, respectively, as shown in Figure 1. For simplicity, V_x and V_y are assumed to be constant along the cable, although their variation can be incorporated in the analysis without any substantial modification. We also neglect the tangential drag on the cable. Incorporating the effect of damping/drag-forces and retaining only linear terms for small-amplitude dynamic motion, the governing equations of motion are obtained as

$$\frac{\partial}{\partial s}\left\{\frac{T_s}{1+T_s/EA}\frac{\partial v_t}{\partial s} + \frac{EA}{(1+T_s/EA)^3}\frac{\mathrm{d}y}{\mathrm{d}s}\left(\frac{\mathrm{d}x}{\mathrm{d}s}\frac{\partial u_t}{\partial s} + \frac{\mathrm{d}y}{\mathrm{d}s}\frac{\partial v_t}{\partial s}\right)\right\}$$
$$= \frac{\partial}{\partial t}\left\{m(s)\frac{\partial v_t}{\partial t}\right\} + C_n^d(s)\left|\left[\left(V_y - \frac{\partial v_t}{\partial t}\right)^2 + \left(V_x - \frac{\partial u_t}{\partial t}\right)^2\right]^{1/2}\right|\left(V_y - \frac{\partial v_t}{\partial t}\right) + C_v^s(s)\frac{\partial v_t}{\partial t}, \tag{8}$$

$$\frac{\partial}{\partial s}\left\{\frac{T_s}{1+T_s/EA}\frac{\partial u_t}{\partial s} + \frac{EA}{(1+T_s/EA)^3}\frac{\mathrm{d}x}{\mathrm{d}s}\left(\frac{\mathrm{d}x}{\mathrm{d}s}\frac{\partial u_t}{\partial s} + \frac{\mathrm{d}y}{\mathrm{d}s}\frac{\partial v_t}{\partial s}\right)\right\}$$
$$= \frac{\partial}{\partial t}\left\{m(s)\frac{\partial u_t}{\partial t}\right\} + C_n^d(s)\left|\left[\left(V_y - \frac{\partial v_t}{\partial t}\right)^2 + \left(V_x - \frac{\partial u_t}{\partial t}\right)^2\right]^{1/2}\right|\left(V_x - \frac{\partial u_t}{\partial t}\right) + C_u^s(s)\frac{\partial u_t}{\partial t}. \tag{9}$$

In this analysis, a relative velocity form of drag loading is assumed. It should be noted that the drag-force terms contain mean components (to be determined iteratively in the framework of statistical linearization, as explained in the subsequent sections) due to the presence of the current velocities V_x and V_y. Consequently, the total dynamic displacements v_t and u_t will contain mean offsets v_s and u_s, and zero-mean dynamic components v and u.

3. DYNAMIC STIFFNESS APPROACH

To perform the frequency-domain analysis, the nonlinear drag-force is linearized by the well-known equivalent linearization technique (Roberts & Spanos 1990). When harmonic excitation at frequency ω acts on the cable, the system being linearized, all points oscillate harmonically at the frequency ω. One can therefore take $u(s,t) = \mathscr{R}e[u(s)\exp(\mathrm{i}\omega t)]$ and $v(s,t) = \mathscr{R}e[v(s)\exp(\mathrm{i}\omega t)]$. Consequently, the equations governing $u(s)$ and $v(s)$ can be shown to be given by

$$\frac{\mathrm{d}}{\mathrm{d}s}\left[\left\{\frac{T_s}{1+T_s/EA}+\frac{EA}{(1+T_s/EA)^3}\left(\frac{\mathrm{d}y}{\mathrm{d}s}\right)^2\right\}\frac{\mathrm{d}v}{\mathrm{d}s}+\left\{\frac{EA}{(1+T_s/EA)^3}\frac{\mathrm{d}y}{\mathrm{d}s}\frac{\mathrm{d}x}{\mathrm{d}s}\right\}\frac{\mathrm{d}u}{\mathrm{d}s}\right]$$
$$=[-m\omega^2+\mathrm{i}\omega\{B_1(s)+C_v^s\}]v, \tag{10}$$

$$\frac{\mathrm{d}}{\mathrm{d}s}\left[\left\{\frac{T_s}{1+T_s/EA}+\frac{EA}{(1+T_s/EA)^3}\left(\frac{\mathrm{d}x}{\mathrm{d}s}\right)^2\right\}\frac{\mathrm{d}u}{\mathrm{d}s}+\left\{\frac{EA}{(1+T_s/EA)^3}\frac{\mathrm{d}y}{\mathrm{d}s}\frac{\mathrm{d}x}{\mathrm{d}s}\right\}\frac{\mathrm{d}v}{\mathrm{d}s}\right]$$
$$=[-m\omega^2+\mathrm{i}\omega\{B_2(s)+C_u^s\}]u, \tag{11}$$

where $B_1(s)$ and $B_2(s)$ are the linearized drag-damping coefficients along the cable. To deal with the random excitations, equations (10) and (11) are to be solved for each frequency where the excitation energy is present. Consequently, the frequency response functions of the cable can be obtained to perform spectral analysis. A number of methods for stochastic linearization of two- and three-dimensional drag-forces are available, which are based on mean-square error minimization and invariant properties of drag-forces (Leira 1987). In the present analysis, we neglect the chordwise relative velocity, and assume a shallow-sag cable ($B_2 = 0$), making the drag force one-dimensional. Assuming Gaussian response, the equivalent linear form of drag force is given by (Malhotra & Penzien 1970; Wu & Tung 1975; Paulling 1979)

$$C_v^d(s)\left|\left(V_y-\frac{\partial v}{\partial t}\right)\right|\left(V_y-\frac{\partial v}{\partial t}\right)\equiv B_1(s)\frac{\partial v}{\partial t}+\tilde{F}_d(s), \tag{12}$$

where

$$B_1(s)=\sqrt{\frac{8}{\pi}}\,C_v^d(s)\left\{\sigma_{\dot v}\exp\left[-\frac{1}{2}\left(\frac{V_y}{\sigma_{\dot v}}\right)^2\right]+\sqrt{2\pi}V_y\,\mathrm{erf}\left(\frac{V_y}{\sigma_{\dot v}}\right)\right\}, \tag{13}$$

$$\tilde{F}_d(s)=\sqrt{\frac{2}{\pi}}\,C_v^d(s)\left\{V_y\sigma_{\dot v}\exp\left[-\frac{1}{2}\left(\frac{V_y}{\sigma_{\dot v}}\right)^2\right]+\sqrt{2\pi}(\sigma_{\dot v}^2+V_y^2)\,\mathrm{erf}\left(\frac{V_y}{\sigma_{\dot v}}\right)\right\} \tag{14}$$

and

$$C_v^d(s)=\left(\frac{\mathrm{d}x}{\mathrm{d}s}\right)^2 C_n^d(s),\qquad \sigma_{\dot v}^2=E[\dot v(s)^2],\qquad \mathrm{erf}(x)=\frac{1}{\sqrt{2\pi}}\int_0^x |\mathrm{e}|^{-1/2y^2}\,\mathrm{d}y.$$

The dynamic part of the linearized drag-force (related to B_1) is considered in equation (10). The mean equivalent drag-force $\bar{F}_d$ will be used to obtain the mean dynamic

displacements v_s and u_s. The equations governing v_s and u_s can be obtained by replacing the right-hand sides of equations (10) and (11) by $\bar{F}_d(s)$ and zero, respectively. It should be noted that the zero-mean dynamic components v and u are coupled with the mean components v_s and u_s through the mean drag term $\bar{F}_d$. The coefficients B_1 and $\bar{F}_d$ can be obtained by iterating until convergence is achieved. It should also be noted that $\bar{F}_d$ is zero in the absence of the current V_y. Thus, the mean offsets v_s and u_s are also then zero. Under the assumption of small V_x and V_y, the mean offsets v_s and u_s due to the mean drag-force $\bar{F}_d$ are insignificant compared with the initial static deflection due to gravity (in the absence of current). For higher current velocities, the nonlinear terms in v_s and u_s need to be retained to obtain the equations for the mean dynamic displacements, leading to nonlinear partial differential equations. These equations will also be coupled with the linear differential equations governing the zero-mean dynamic displacements. To solve the resulting complex problem, the drag-force can be approximated as $C_v^d(s)|(V_y - \partial v/\partial t)|(V_y - \partial v/\partial t) \approx C_v^d(s)|V_y|V_y + C_v^d(s)|\partial v/\partial t|(\partial v/\partial t)$. This commonly used approximation simplifies the calculations of the mean components v_s and u_s (now uncoupled from v and u) which can then be used to update the initial configuration $x(s)$ and $y(s)$ used to determine the zero-mean dynamic displacements v and u in equations (10) and (11).

It is also worth mentioning that the same procedure can be extended directly to consider the general case of drag forces for a cable with large sag [given in equations (8) and (9)]. However, this is algebraically more involved. As the purpose of the paper is to illustrate the numerical scheme, we consider only the simple case of the one-dimensional drag-force.

Next, the method developed by Sarkar & Manohar (1996) is applied to solve the above pair of equations for given displacement boundary conditions. The boundary conditions on displacements are specified as

$$v(0) = 0; \quad v(L) = \Delta_{Rv} + \mathrm{i}\Delta_{Iv}; \quad u(0) = 0; \quad u(L) = \Delta_{Ru} + \mathrm{i}\Delta_{Iu}, \tag{15}$$

where Δ_{Rv} and Δ_{Iv} are the real and imaginary parts of $v(L)$. Similarly, Δ_{Ru} and Δ_{Iu} are the real and imaginary parts of $u(L)$.

Equations (10) and (11) constitute a set of complex boundary value problems with nonhomogeneous boundary conditions. They can be recast into a set of eight first-order real equations, by introducing the variables $y_k(s)$, $k = 1, 2, \ldots, 8$ through the relations:

$$v(s) = y_1(s) + \mathrm{i}y_2(s),$$

$$u(s) = y_3(s) + \mathrm{i}y_4(s),$$

$$\left[\left\{\frac{T_s}{1 + T_s/EA} + \frac{EA}{(1 + T_s/EA)^3}\left(\frac{\mathrm{d}y}{\mathrm{d}s}\right)^2\right\}\frac{\mathrm{d}v}{\mathrm{d}s} + \left\{\frac{EA}{(1 + T_s/EA)^3}\frac{\mathrm{d}y}{\mathrm{d}s}\frac{\mathrm{d}x}{\mathrm{d}s}\right\}\frac{\mathrm{d}u}{\mathrm{d}s}\right] = y_5(s) + \mathrm{i}y_6(s),$$

$$\left[\left\{\frac{T_s}{1 + T_s/EA} + \frac{EA}{(1 + T_s/EA)^3}\left(\frac{\mathrm{d}x}{\mathrm{d}s}\right)^2\right\}\frac{\mathrm{d}u}{\mathrm{d}s} + \left\{\frac{EA}{(1 + T_s/EA)^3}\frac{\mathrm{d}y}{\mathrm{d}s}\frac{\mathrm{d}x}{\mathrm{d}s}\right\}\frac{\mathrm{d}v}{\mathrm{d}s}\right] = y_7(s) + \mathrm{i}y_8(s).$$

Substituting these equations into equations (10) and (11), and separating real and imaginary parts, one obtains

$$\left[\left\{\frac{T_s}{1 + T_s/EA} + \frac{EA}{(1 + T_s/EA)^3}\left(\frac{\mathrm{d}y}{\mathrm{d}s}\right)^2\right\}\frac{\mathrm{d}y_1}{\mathrm{d}s} + \left\{\frac{EA}{(1 + T_s/EA)^3}\frac{\mathrm{d}y}{\mathrm{d}s}\frac{\mathrm{d}x}{\mathrm{d}s}\right\}\frac{\mathrm{d}y_3}{\mathrm{d}s}\right] - y_5(s) = 0,$$

$$\left[\left\{\frac{T_s}{1 + T_s/EA} + \frac{EA}{(1 + T_s/EA)^3}\left(\frac{\mathrm{d}y}{\mathrm{d}s}\right)^2\right\}\frac{\mathrm{d}y_2}{\mathrm{d}s} + \left\{\frac{EA}{(1 + T_s/EA)^3}\frac{\mathrm{d}y}{\mathrm{d}s}\frac{\mathrm{d}x}{\mathrm{d}s}\right\}\frac{\mathrm{d}y_4}{\mathrm{d}s}\right] - y_6(s) = 0,$$

$$\left[\left\{\frac{T_s}{1+T_s/EA}+\frac{EA}{(1+T_s/EA)^3}\left(\frac{\mathrm{d}x}{\mathrm{d}s}\right)^2\right\}\frac{\mathrm{d}y_3}{\mathrm{d}s}+\left\{\frac{EA}{(1+T_s/EA)^3}\frac{\mathrm{d}y}{\mathrm{d}s}\frac{\mathrm{d}x}{\mathrm{d}s}\right\}\frac{\mathrm{d}y_1}{\mathrm{d}s}\right]-y_7(s)=0,$$

$$\left[\left\{\frac{T_s}{1+T_s/EA}+\frac{EA}{(1+T_s/EA)^3}\left(\frac{\mathrm{d}x}{\mathrm{d}s}\right)^2\right\}\frac{\mathrm{d}y_4}{\mathrm{d}s}+\left\{\frac{EA}{(1+T_s/EA)^3}\frac{\mathrm{d}y}{\mathrm{d}s}\frac{\mathrm{d}x}{\mathrm{d}s}\right\}\frac{\mathrm{d}y_2}{\mathrm{d}s}\right]-y_8(s)=0,$$

$$\frac{\mathrm{d}y_5}{\mathrm{d}s}+m\omega^2y_1+\omega(B_1+C_v^s)y_2=0,$$

$$\frac{\mathrm{d}y_6}{\mathrm{d}s}+m\omega^2y_2-\omega(B_1+C_v^s)y_1=0,$$

$$\frac{\mathrm{d}y_7}{\mathrm{d}s}+m\omega^2y_3+\omega(B_2+C_u^s)y_4=0,$$

$$\frac{\mathrm{d}y_8}{\mathrm{d}s}+m\omega^2y_4-\omega(B_2+C_u^s)y_3=0.$$

These equations can be recast in the form

$$\mathbf{y}'=\mathbf{A}\mathbf{y}. \tag{16}$$

The prime here denotes the derivative with respect to s, and $\mathbf{A}$ is an 8×8 matrix whose elements are functions of s. A closed-form solution is not available for these equations. Consequently, the boundary value problem is converted into a set of equivalent initial value problems, and spatial marching techniques are applied to obtain the numerical solution.

3.1. Equivalent Set of Initial Value Problems

A matrix of fundamental solutions of equation (16), denoted by $\mathbf{W}(s)$, is obtained by solving this equation under the *initial* conditions

$$W_{ij}(s=0)=\delta_{ij}, \tag{17}$$

where δ_{ij} is the Kronecker delta function. Any other solution $\mathbf{y}(s)$ of equation (16) can be written as a linear combination of the elements of $\mathbf{W}(s)$,

$$\mathbf{y}(s)=\mathbf{W}(s)\boldsymbol{\alpha}, \tag{18}$$

where the vector $\boldsymbol{\alpha}$ needs to be selected to satisfy the prescribed boundary conditions on displacements. Thus, for the displacement boundary conditions, one obtains

$$\begin{Bmatrix}\Delta_{Rv}(0)\\ \Delta_{Iv}(0)\\ \Delta_{Ru}(0)\\ \Delta_{Iu}(0)\\ \Delta_{Rv}(L)\\ \Delta_{Iv}(L)\\ \Delta_{Ru}(L)\\ \Delta_{Iu}(L)\end{Bmatrix}=\begin{bmatrix}1 & 0 & 0 & 0 & 0 & 0 & 0 & 0\\ 0 & 1 & 0 & 0 & 0 & 0 & 0 & 0\\ 0 & 0 & 1 & 0 & 0 & 0 & 0 & 0\\ 0 & 0 & 0 & 1 & 0 & 0 & 0 & 0\\ W_{11}(L) & W_{12}(L) & W_{13}(L) & W_{14}(L) & W_{15}(L) & W_{16}(L) & W_{17}(L) & W_{18}(L)\\ W_{21}(L) & W_{22}(L) & W_{23}(L) & W_{24}(L) & W_{25}(L) & W_{26}(L) & W_{27}(L) & W_{28}(L)\\ W_{31}(L) & W_{32}(L) & W_{33}(L) & W_{34}(L) & W_{35}(L) & W_{36}(L) & W_{37}(L) & W_{38}(L)\\ W_{41}(L) & W_{42}(L) & W_{43}(L) & W_{44}(L) & W_{45}(L) & W_{46}(L) & W_{47}(L) & W_{48}(L)\end{bmatrix}\begin{Bmatrix}\alpha_1\\ \alpha_2\\ \alpha_3\\ \alpha_4\\ \alpha_5\\ \alpha_6\\ \alpha_7\\ \alpha_8\end{Bmatrix}. \tag{19}$$

Similarly, from the boundary forces one gets

$$\begin{Bmatrix} p_{Rv}(0) \\ p_{Iv}(0) \\ p_{Ru}(0) \\ p_{Iu}(0) \\ p_{Rv}(L) \\ p_{Iv}(L) \\ p_{Ru}(L) \\ p_{Iu}(L) \end{Bmatrix} = \begin{bmatrix} 0 & 0 & 0 & 0 & 1 & 0 & 0 & 0 \\ 0 & 0 & 0 & 0 & 0 & 1 & 0 & 0 \\ 0 & 0 & 0 & 0 & 0 & 0 & 1 & 0 \\ 0 & 0 & 0 & 0 & 0 & 0 & 0 & 1 \\ W_{51}(L) & W_{52}(L) & W_{53}(L) & W_{54}(L) & W_{55}(L) & W_{56}(L) & W_{57}(L) & W_{58}(L) \\ W_{61}(L) & W_{62}(L) & W_{63}(L) & W_{64}(L) & W_{65}(L) & W_{66}(L) & W_{67}(L) & W_{68}(L) \\ W_{71}(L) & W_{72}(L) & W_{73}(L) & W_{74}(L) & W_{75}(L) & W_{76}(L) & W_{77}(L) & W_{78}(L) \\ W_{81}(L) & W_{82}(L) & W_{83}(L) & W_{84}(L) & W_{85}(L) & W_{86}(L) & W_{87}(L) & W_{88}(L) \end{bmatrix} \begin{Bmatrix} \alpha_1 \\ \alpha_2 \\ \alpha_3 \\ \alpha_4 \\ \alpha_5 \\ \alpha_6 \\ \alpha_7 \\ \alpha_8 \end{Bmatrix}. \tag{20}$$

For the specific case shown in Figure 1, the mooring cable is subjected to support excitation on its right-hand end whereas the left-hand end is fixed at the ocean floor. In this case, the first four elements in vector α are zero. The remaining nonzero elements satisfy the following equation:

$$\begin{Bmatrix} \Delta_{Rv} \\ \Delta_{Iv} \\ \Delta_{Ru} \\ \Delta_{Iu} \end{Bmatrix} = \begin{bmatrix} W_{15}(L) & W_{16}(L) & W_{17}(L) & W_{18}(L) \\ W_{25}(L) & W_{26}(L) & W_{27}(L) & W_{28}(L) \\ W_{35}(L) & W_{36}(L) & W_{37}(L) & W_{38}(L) \\ W_{45}(L) & W_{46}(L) & W_{47}(L) & W_{48}(L) \end{bmatrix} \begin{Bmatrix} \alpha_5 \\ \alpha_6 \\ \alpha_7 \\ \alpha_8 \end{Bmatrix}. \tag{21}$$

In compact form, we have

$$\mathbf{\Delta}_L = \mathbf{W}_L \tilde{\boldsymbol{\alpha}}. \tag{22}$$

From equation (18), the following relation can be obtained for the response of any intermediate point in the cable:

$$\begin{Bmatrix} y_1(s) \\ y_2(s) \\ y_3(s) \\ y_4(s) \end{Bmatrix} = \begin{bmatrix} W_{15}(s) & W_{16}(s) & W_{17}(s) & W_{18}(s) \\ W_{25}(s) & W_{26}(s) & W_{27}(s) & W_{28}(s) \\ W_{35}(s) & W_{36}(s) & W_{37}(s) & W_{38}(s) \\ W_{45}(s) & W_{46}(s) & W_{47}(s) & W_{48}(s) \end{bmatrix} \begin{Bmatrix} \alpha_5 \\ \alpha_6 \\ \alpha_7 \\ \alpha_8 \end{Bmatrix}. \tag{23}$$

In concise form, we have

$$\mathbf{Y}_S = \mathbf{W}_S \tilde{\boldsymbol{\alpha}}. \tag{24}$$

From equation (22) and (24), we get

$$\mathbf{Y}_S = \mathbf{W}_S \mathbf{W}_L^{-1} \mathbf{\Delta}_L \tag{25}$$

or, introducing the matrix $\mathbf{R}$, we can write

$$\mathbf{Y}_S = \mathbf{R}\mathbf{\Delta}_L. \tag{26}$$

The equation relating the response at any intermediate point to the prescribed boundary displacements X (surge) and Y (heave) can be expressed as

$$\begin{Bmatrix} v(s) \\ u(s) \end{Bmatrix} = \begin{bmatrix} (R_{11} + \mathrm{i}R_{12}) & (R_{13} + \mathrm{i}R_{14}) \\ (R_{31} + \mathrm{i}R_{32}) & (R_{33} + \mathrm{i}R_{34}) \end{bmatrix} \begin{bmatrix} \cos\theta & -\sin\theta \\ \sin\theta & \cos\theta \end{bmatrix} \begin{Bmatrix} X \\ Y \end{Bmatrix}, \tag{27}$$

which can be written as

$$\mathbf{U(s)} = \mathbf{FX}, \tag{28}$$

where $\mathbf{F}$ is a 2×2 transfer matrix relating the intermediate displacement vector $\mathbf{U}$ to the vector $\mathbf{X}$ of the imposed displacements at the end of the cable.

Let us assume that the power spectral density matrix $\mathbf{S}(\omega)$ of the boundary excitations is given by

$$\mathbf{S}(\omega) = \begin{bmatrix} S_{xx}(\omega) & S_{xy}(\omega) \\ S_{yx}(\omega) & S_{yy}(\omega) \end{bmatrix}. \tag{29}$$

The response variances of $v(s, t)$ are then given by

$$\sigma_v^2(s) = \int_{\omega_1}^{\omega_2} [S_{xx}(\omega)H_{vx}(\omega) + S_{yy}(\omega)H_{vy}(\omega) + 2\mathscr{R}e\{S_{xy}(\omega)H_{vxy}(\omega)\}]\,\mathrm{d}\omega, \tag{30}$$

where

$$H_{vx} = |F_{11}|^2, \quad H_{vy} = |F_{12}|^2, \quad H_{vxy} = F_{11}\bar{F}_{12}.$$

Here the bar indicates the complex conjugate. Similar expressions can be derived for any other response quantity such as dynamic cable tension, etc. Typical results are given in Section 5.

3.2. Additional Consideration of Point and Distributed Loads as Particular Integrals

The method is capable of handling the effect of distributed or lumped disturbances in terms of a particular integral. To illustrate this point, we can consider a cable carrying a concentrated harmonic load with amplitude Q at a point s_0. To obtain the particular integral, the solution of equation (16) is obtained with initial condition $\mathbf{y}(0)^* = [0,\ 0,\ 0,\ 0,\ 1,\ 0,\ 0,\ 0]$, where * denotes matrix transposition. This is in fact the impulse response function, which when convolved with the external excitation leads to the desired solution. This function, $\mathbf{y}_5(x)$, is the fifth column of the matrix $\mathbf{W}$ in equation (18). The total solution can now be written as (Sarkar & Manohar 1996)

$$\begin{aligned} \mathbf{y}(s) &= \mathbf{W}(s)\boldsymbol{\alpha}, \quad s \le s_0 \\ &= \mathbf{W}(s)\boldsymbol{\alpha} + Q\int_{s_0}^{x} \mathbf{y}_5(s-\tau)\delta(\tau - s_0)\,\mathrm{d}\tau, \quad s \ge s_0. \end{aligned} \tag{31}$$

This formulation can be directly generalized to include the effects of distributed disturbances, in which case the convolution with the system impulse function has to be carried out numerically. The spatial discretization of a distributed parameter system is significantly influenced by the presence of such effects when the finite-difference or finite-element method is used.

4. OUT-OF-PLANE MOTION: EFFECT OF SEABED FRICTION ON DRAG DAMPING

Catenary mooring cables often have a significant length lying on the ocean floor, giving rise to frictional forces. Following Liu & Bergdahl (1997a), a Coulomb damping model has been chosen here to represent the soil friction which resists the motion of the cable. Moreover, it is quite reasonable to assume that out-of-plane motion of the cable will give rise to more significant frictional damping than in-plane motion, as mooring cables are generally stiff in the axial direction. Ignoring any out-of-plane component of current, the coupling between in-plane and out-of-plane displacements is neglected. Also neglected is the coupling between in-plane and out-of-plane motions, due to the off-diagonal terms in the linearized

drag-damping matrix which can arise when more accurate methods of multidimensional drag-force linearization (Leira 1987) are adopted. The out-of-plane motion of the cable is now governed by the equation of motion of a transversely vibrating string. The effect of lifting-off is neglected by assuming small-amplitude planar motion. This assumes that the portion of the cable lying on the seabed does not change with time. Furthermore, Morison's equation for the drag-force is assumed to be valid even for the portion of the cable in contact with the seafloor. Consequently, the equation of motion of the out-of-plane displacement $w(s,t)$ is given by

$$\frac{\partial}{\partial s}\left\{T_s(s)\frac{\partial w}{\partial s}\right\} = \frac{\partial}{\partial t}\left\{m(s)\frac{\partial w}{\partial t}\right\} + C_w^d(s)\left|\frac{\partial w}{\partial t}\right|\frac{\partial w}{\partial t} + \mu mg\frac{\partial w/\partial t}{|\partial w/\partial t|}\cup(L_s - s). \tag{32}$$

The term L_s denotes the length of the portion of the cable on the seabed, μ is the kinematic coefficient of friction between the seabed and the cable, $C_w^d = \frac{1}{2}\rho_w C_d d$, and $\cup$ represents the unit step function indicating that the frictional force acts only on that part of the cable which lies on the seabed. By linearizing the fluid drag and frictional force, one can express the equation of motion in the frequency domain as

$$\frac{\mathrm{d}}{\mathrm{d}s}\left[T_s(s)\frac{\mathrm{d}w}{\mathrm{d}s}\right] = [-m\omega^2 + \mathrm{i}\omega B_3(s)]w, \tag{33}$$

where $B_3(s)$ is the linearized damping coefficient. Assuming that the response is Gaussian, the distribution of the linearized damping $B_3(s)$ can be expressed as

$$B_3(s) = \underbrace{\sqrt{\frac{8}{\pi}}\,C_w^d\sigma_{\dot{w}}}_{B_{3d}} + \underbrace{\sqrt{\frac{2}{\pi}}\,\frac{\mu mg}{\sigma_{\dot{w}}}\cup(L_s - s)}_{B_{3f}} \tag{34}$$

Following a similar procedure to that outlined in Section 3, the linearized damping $B_3(s)$ can be determined iteratively. In the next section, numerical results are presented which show the influence of the seabed friction on the hydrodynamic drag acting on a mooring cable.

5. NUMERICAL RESULTS

A computer program, based on the work of Sarkar & Manohar (1996), has been extended to incorporate the above analysis. To validate the program, the following checks have been made.

(i) Matching the natural frequencies with results for a cable reported in the literature (Sarkar & Manohar 1996).
(ii) Satisfaction of reciprocity requirements of the system transfer function and symmetry properties of the dynamic stiffness coefficients.†
(iii) Observation of the well-known qualitative features of resonances, antiresonances and minima of direct and cross-receptance functions.

† The dynamic stiffness coefficient between two points is defined as the amplitude of a harmonic force of frequency ω applied at one point which is required to produce a unit harmonic displacement at frequency ω at the other point (Paz 1985).

(iv) Comparison with the closed-form solution for a uniformly damped string. If the acceleration due to gravity is set to zero in the cable equations, the sag of the cable becomes zero and it behaves like a string in its transverse vibrations. Further, if the damping (B_1) is assumed to be uniform along the length as an initial guess, the following closed-form solution relates the spectrum of response to that of excitation at any point on a horizontal cable ($\theta = 0$) in the first iteration (see equation (13) for the case of zero current):

$$S_v(\omega) = \left|\frac{\sin(\alpha s)}{\sin(\alpha L)}\right|^2 S_{xx}(\omega), \tag{35}$$

$$S_{\dot{v}}(\omega) = \omega^2 \left|\frac{\sin(\alpha s)}{\sin(\alpha L)}\right|^2 S_{xx}(\omega), \tag{36}$$

where

$$\alpha^2 = \frac{(-m\omega^2 + \mathrm{i}\omega B_1)}{T_s}. \tag{37}$$

From these relations, the r.m.s. velocity response ($\sigma_{\dot{v}}$) can be calculated along the length of the string. The damping (B_1) obtained in the first iteration by this relation is compared with that obtained by the computer program based on the numerical method.

For the base case, the following parameters for the mooring chain are specified: $EA = 5 \times 10^8$ N, $m = 135{\cdot}35$ kg/m, $\theta = 30^\circ$, $L = 1000$ m, g = 9·807 m/s^2, $\rho_w = 1040$ kg/m^3, $C_d = 1$, $d = 76$ mm, $H_0 = 1{\cdot}0 \times 10^6$ N. Both of the excitation autospectra, S_{xx} and S_{yy}, are taken to be band-limited white-noise. The excitations are assumed to be independent ($S_{xy} = 0$). The current velocity is zero. Using a fifth-order Runge–Kutta scheme, an integration step size of $L/200$ is found to give satisfactory results for all the cases considered below. The iterations are generally observed to converge within four to seven cycles for the cases examined here. Figure 2 shows the comparison between the analytical and numerical results for the distribution of the damping $B_1(s)$ for a string obtained in the first iteration. In this

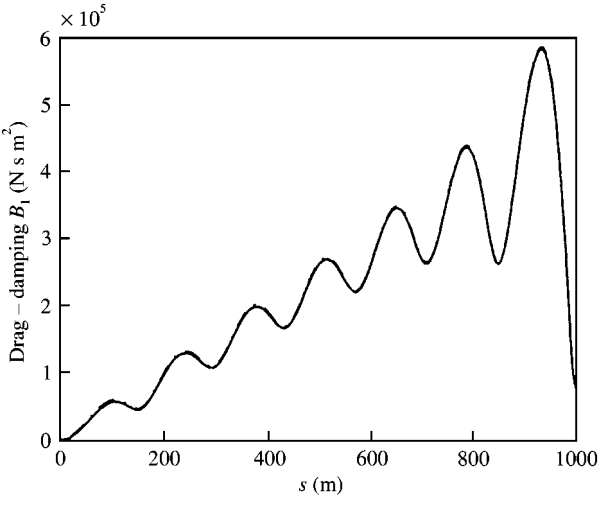

Figure 2. Comparison between analytical and numerical solution: ——, *analytical* and – · – · –, *numerical.*

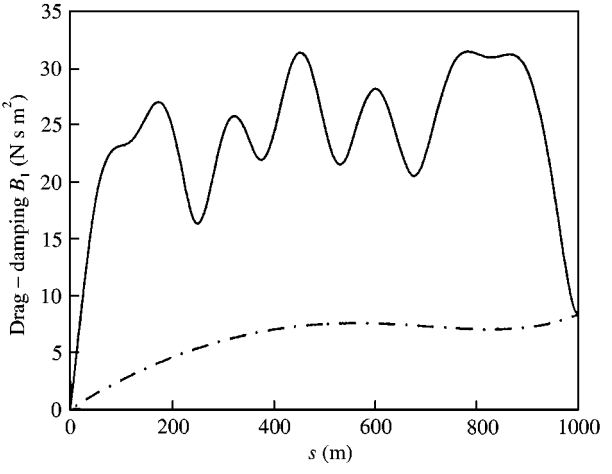

Figure 3. Effect of dynamic and quasistatic analysis: ——, *dynamic*; – · – · –, *quasistatic*.

case, $B_1(s)$ is assumed be uniform along the length as an initial guess, and acceleration due to gravity is set to zero which reduces the cable dynamic equation to the equation of motion of a tranversely vibrating string. The results show excellent agreement.

Next, the effect on drag damping of varying the various system parameters independently is studied.

5.1. Effect of Dynamic and Quasistatic Analysis

The distribution of the drag damping along the cable for the dynamic and quasistatic cases is shown in Figure 3. The frequency range of the excitation is 0·5–2·0 rad/s and the variance is 0·2 m^2. Only surge motion of the free end of the cable is considered. The quasistatic case is simulated assuming a small value of the mass/unit length m ($= 0{\cdot}1$ kg/m) in the computer program developed for the dynamic analysis. It can be seen that the dynamic magnification significantly increases the drag damping for the case considered here. This fact indicates the necessity of including cable dynamics and also points towards the limitation of the quasistatic analysis in calculating the drag damping.

5.2. Effect of Excitation Bandwidth

The excitation is considered to be spread over three different ranges of frequency, but with the same variance 0·1 m^2 and central frequency 1·5 rad/s. The three ranges are 0·5–2·5, 1–2 and 1·25–1·75 rad/s. Figure 4 illustrates the results for surge motion. Figure 4(a) shows the damping profiles for the different excitation bandwidths. The most narrow-banded excitation generates the highest damping. The irregularities in the drag-damping profile tend to increase with the decrease in the bandwidth of the excitation. For excitations with broader bandwidth, several modes contribute significantly to the total response, thereby making the damping profile smoother along the cable. Conversely, only a few modes appear to make the major contributions to the total response for narrow-banded excitation, and thus seem to give rise to a relatively more irregular damping profile. Figures 4(b) and 4(c) present the power spectral density of $v(s, t)$ and the dynamic cable tension at the midspan of the cable.

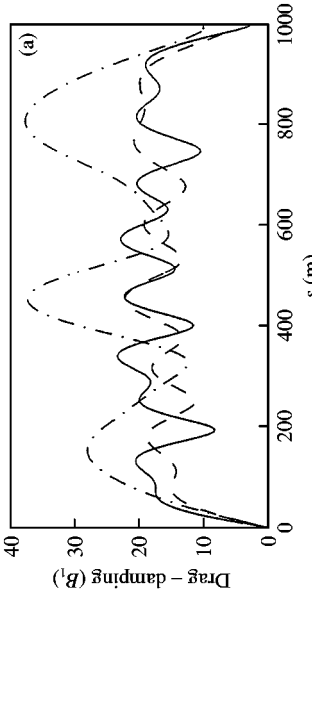

Figure 4. Effect of excitation bandwidth on surge response: ——, $(\omega_1, \omega_2) = 0{\cdot}5$–$2{\cdot}5$ rad/s; – – –, $(\omega_1, \omega_2) = 1$–2 rad/s and –·–·–, $(\omega_1, \omega_2) = 1{\cdot}25$–$1{\cdot}75$ rad/s. (a) Drag damping in N s m^2; (b) $S_v(\omega)$ in m^2 rad^{-1} and (c) $S_{tension}(\omega)$ in N^2 rad^{-1}.

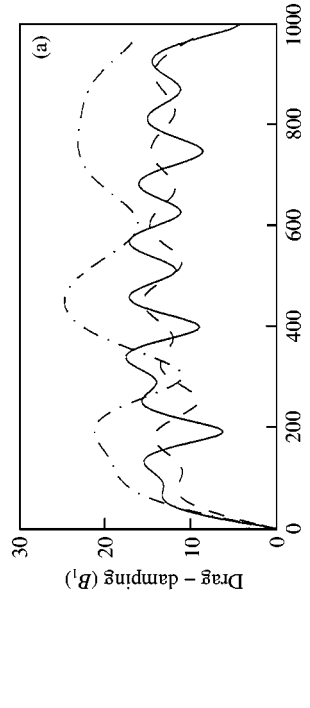

Figure 5. Effect of excitation bandwidth on heave response: ——, $(\omega_1, \omega_2) = 0{\cdot}5$–$2{\cdot}5$ rad/s; – – –, $(\omega_1, \omega_2) = 1$–2 rad/s and –·–·–, $(\omega_1, \omega_2) = 1{\cdot}25$–$1{\cdot}75$ rad/s. (a) Drag damping in N s m^2; (b) $S_v(\omega)$ in m^2 rad^{-1} and (c) $S_{tension}(\omega)$ in N^2 rad^{-1}.

Although the amplitude of the power spectral densities increases with the decrease in the excitation bandwidth, the response variance still decreases. This is evident considering the areas under the power spectral densities in Figures 4(b) and 4(c). Similar results are shown in Figure 5 for the case of heave excitation.

5.3. Effect of Amplitude of Excitation

Three different excitation variances are considered: 0·1, 0·2 and 0·3 m^2. For surge excitations, Figure 6(a-c) presents the damping profiles, the power spectral densities of $v(s,t)$ and dynamic cable tension, respectively. Evidently, the excitation with higher amplitude induces higher damping. However, the response amplitudes increase for the higher amplitudes of excitation as is evident from Figures 6(b) and 6(c). Similar trends appear in the case of heave motion, as illustrated in Figure 7.

5.4. Effect of Drag Coefficient

Figure 8(a–c) presents the results for the surge motion (with a variance of 0·1 m^2) for three values of drag coefficients ($C_d = 1$, 1·5 and 2). Evidently, the increase in C_d significantly increases the drag damping as is evident from Figure 8(a). However, the decrease in the response is less dramatic compared to the increase in drag damping, as noted from Figures 7(b) and 7(c) showing the spectra for $v(s,t)$ and dynamic cable tension. For the case of heave response, similar results are shown in Figure 9.

5.5. Effect of Composite Properties and Current

Next, a composite mooring cable is considered. It is assumed to have three parts: two end segments (made of chains), each of length 200 m and properties of type A, and a central segment (made of wire rope) of length 600 m and properties of type B. The segments of type A have the following properties: $EA = 5{\cdot}0 \times 10^8$ N, $m = 135{\cdot}35$ kg/m, $C_d = 1{\cdot}0$, $d = 76$ mm. The segment of type B has the following properties: $EA = 7{\cdot}03 \times 10^7$ N, $m = 175{\cdot}9$ kg/m, $C_d = 1{\cdot}0$, $d = 51$ mm. The tension H_0 is 600 kN. For simplicity, the static tension of the composite line is approximated by equations (6) and (7), assuming an average value of mass distribution m_s. Figure 10 shows the drag-damping distribution for the case of surge excitation with a variance of 0·2 m^2. The excitation frequency ranges from 0·5 to 2·0 rad/s. The drag damping has also been plotted under the assumption that the linearized drag is constant along each of the segments. The segmentwise constant drag is calculated by averaging the standard deviation of the velocity response ($\sigma_{\dot{v}}$) along the length of each segment. The effect of uniform currents of 0·25 and 0·5 m/s on the drag damping B_1 is also shown in Figure 10. The effect of mean drag force (related to $\bar{F}_d$) on the static profile is ignored, assuming the influence of current is negligible with respect to gravity on the static profile for the cases considered. It can be observed that the damping distribution is almost constant on the left end segment when there is a current. This is because the response velocity $\dot{v}(s,t)$ is negligible compared with current V_y in this segment. In this case, the expression for B_1 reduces to $2C_d^v V_y$, and is uniform along the segment length. The power spectral densities of $v(s,t)$ at midspan are shown for these four cases in Figure 11. An important observation from the response power spectral density is that the piecewise constant damping assumption underestimates the total damping. It is also readily apparent that current increases the damping.

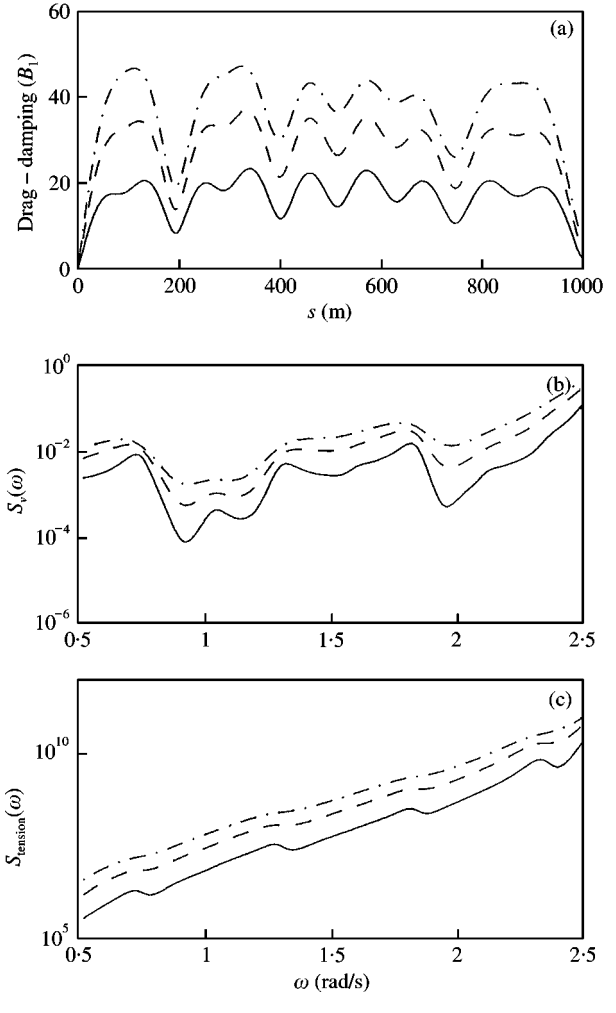

Figure 6. Effect of excitation amplitude on surge response: ——, $S = 0{\cdot}05\ \text{m}^2\ \text{rad}^{-1}$; – – –, $S = 0{\cdot}1\ \text{m}^2\ \text{rad}^{-1}$ and –·–·–, $S = 0{\cdot}15\ \text{m}^2\ \text{rad}^{-1}$. (a) Drag damping in N s m^2; (b) $S_v(\omega)$ in $\text{m}^2\ \text{rad}^{-1}$ and (c) $S_{\text{tension}}(\omega)$ in $\text{N}^2\ \text{rad}^{-1}$.

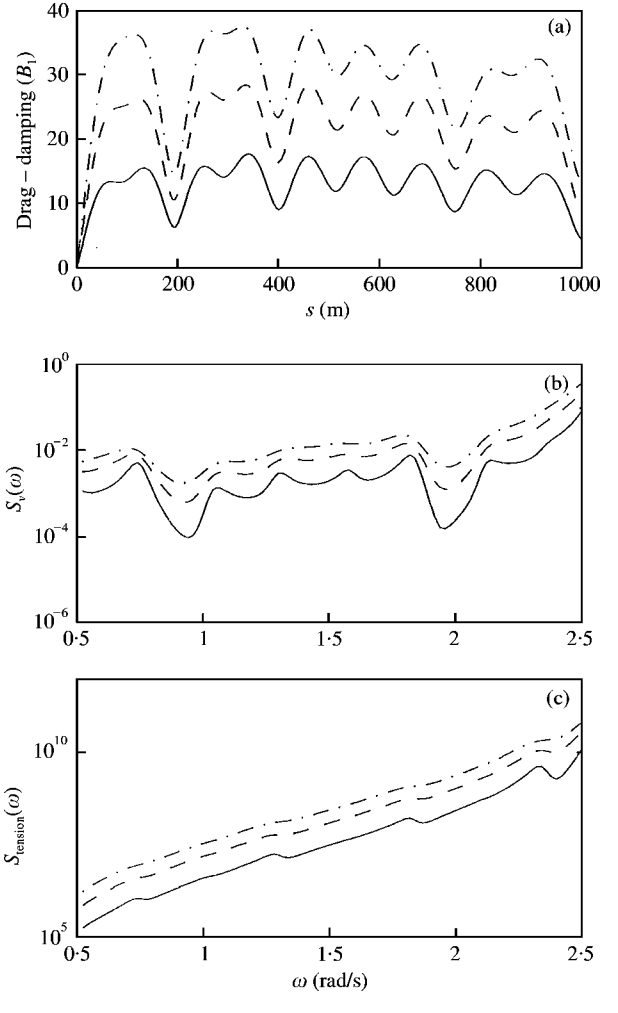

Figure 7. Effect of excitation amplitude on heave response: ——, $S = 0{\cdot}05\ \text{m}^2\ \text{rad}^{-1}$; – – –, $S = 0{\cdot}1\ \text{m}^2\ \text{rad}^{-1}$ and –·–·–, $S = 0{\cdot}15\ \text{m}^2\ \text{rad}^{-1}$. (a) Drag damping in N s m^2; (b) $S_v(\omega)$ in $\text{m}^2\ \text{rad}^{-1}$ and (c) $S_{\text{tension}}(\omega)$ in $\text{N}^2\ \text{rad}^{-1}$.

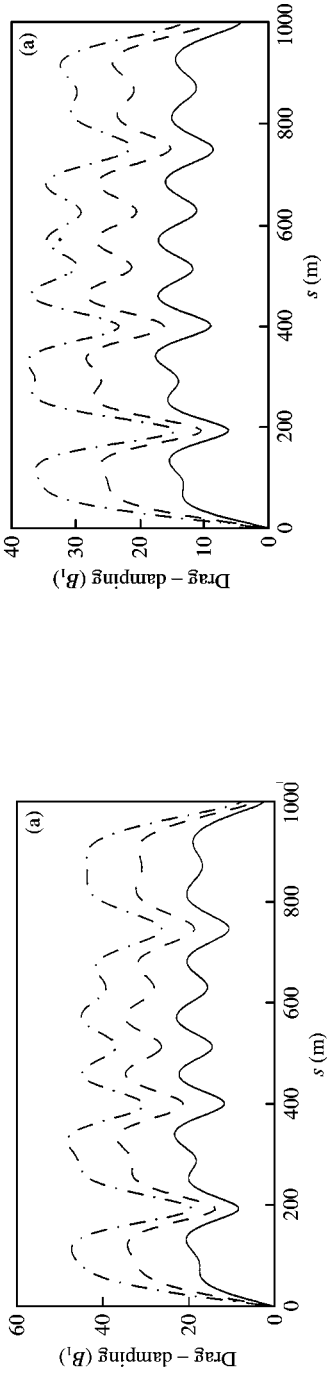

Figure 8. Effect of drag coefficient on surge response: ——, $C_d = 1$; – – –, $C_d = 1{\cdot}5$ and – · – · –, $C_d = 2$. (a) Drag damping in N s m^2; (b) $S_\eta(\omega)$ in m^2 rad^{-1} and (c) $S_{\text{tension}}(\omega)$ in N^2 rad^{-1}.

Figure 9. Effect of drag coefficient on heave response: ——, $C_d = 1$; – – –, $C_d = 1{\cdot}5$ and – · – · –, $C_d = 2$ (a) Drag damping in N s m^2; (b) $S_\eta(\omega)$ in m^2 rad^{-1} and (c) $S_{\text{tension}}(\omega)$ in N^2 rad^{-1}.

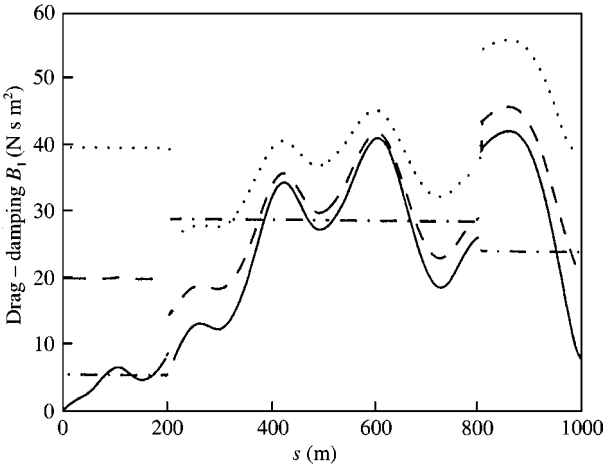

Figure 10. Drag on composite cable ——, actual; –·–·–, segmentwise constant; – – –, current effect ($V_1 = 0{\cdot}25$ m/s) and · · ·, current effect ($V_1 = 0{\cdot}5$ m/s).

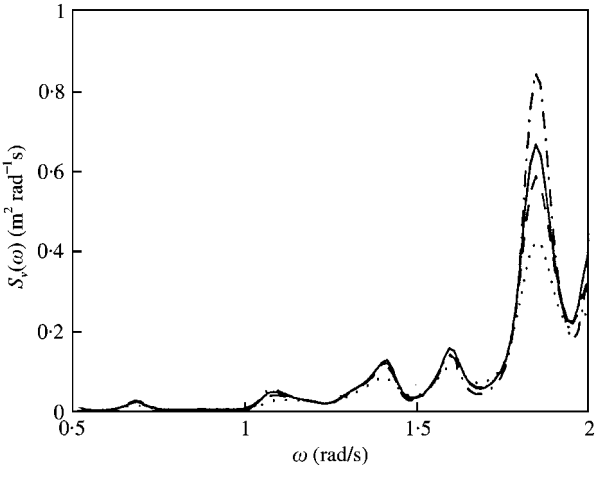

Figure 11. $S_v(\omega)$ at $s = L/2$ for different cases: ——, actual; — · — · —, segmentwise constant; – – –, current effect ($V_1 = 0{\cdot}25$ m/s) and · · ·, current effect ($V_1 = 0{\cdot}5$ m/s).

5.6. Effect of Seabed Friction

A mooring cable (of type A) having total length 1000 m is analysed with a length of 600 m lying on the seabed and subject to frictional forces. The amplitude of excitation is assumed to be small enough so that one can ignore the uplifting effect due to planar motion. The frictional coefficient μ is taken to be 0·3. The excitation is assumed to be band-limited white noise with bandwidth 0·5–2 rad/s and variance 0·05 m^2. Figure 12 shows the linearized drag damping (B_{3d}) and frictional damping (B_{3f}) induced in the cable (i.e., the two terms in equation (34)) due to out-of-plane excitation at the top end. Figure 13 shows the effect of seabed friction on the power spectral density of the out-of-plane displacement $w(s, t)$ at $s = \frac{1}{2}L$. In Figure 12, the drag damping profile is also shown when the effect of seabed friction is neglected. It can be seen that when the seabed friction is neglected, a higher

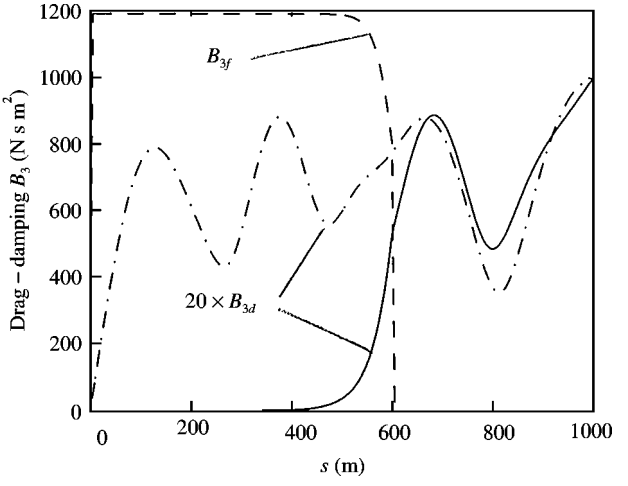

Figure 12. Drag fiction damping: ——, drag damping; – – –, friction damping; –·–·–, drag damping without friction damping.

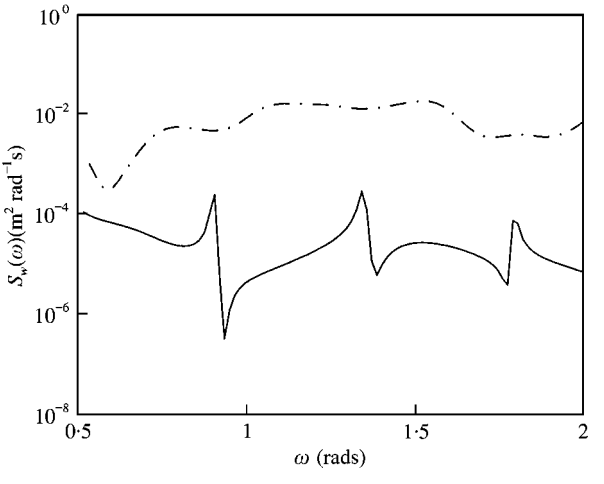

Figure 13. $S_w(\omega)$ at $s = L/2$: ——, with friction damping; –·–·–, without friction damping.

estimate of linearized drag damping is obtained. However, the friction effect significantly reduces the out-of-plane response $w(s, t)$, as shown in Figure 13.

6. CONCLUDING REMARKS

A method of analysing the dynamics of a mooring cable due to random boundary excitations has been described, based on a previously developed technique for dealing with the cable equation. The spatially varying fluid drag has been linearized by statistical linearization. The linearized drag, which is an unknown function of position along the cable, has been determined iteratively. The effect of current velocity on the drag-force has also been studied. The method can analyse the varying material and geometric properties, as in the case of a typical composite mooring cable, in a straightforward manner. It avoids the need for complex eigenvalue analysis, arising due to nonproportional linearized fluid-drag

damping, when finite-element models of mooring lines are solved by modal analysis. Further, while a large number of elements is required to determine the spatial variation of damping using the finite-element method, the present method overcomes this difficulty by directly integrating the equations of motion in the spatial domain. The effect of the seabed interaction has also been investigated using an approximation based on a Coulomb friction model. The technique developed here can also be used for the linear dynamic analysis of towed underwater cables having complex geometry.

From the point of view of previous studies, the present work differs as follows. In the framework of linearized analysis, there is no discretization error involving the solution of the boundary value problem such as is experienced when using finite-difference (Bliek 1984) or finite-element approaches. The solution of the linear boundary value problem is exact, except for the round-off and truncation errors inevitably experienced in the numerical solution of the differential equations. Due to the absence of the discretization error, the present method accurately determines the system eigenvalues (natural frequencies) and eigenfunctions (mode shapes). The approach also avoids the need for carrying out complex eigenvalue analysis due to nonproportionality in the damping. The subsequent response estimation by modal analysis is not corrupted by modal truncation errors. Furthermore, only a few degrees of freedom are adequate for the dynamic analysis of the entire cable. The method is also capable of handling the influence of distributed and point external disturbances, in the form of particular integrals. Finally, the method incorporates a probabilistic approach, for investigating the effect of mooring line damping on the extreme response of a coupled cable and floating vessel assembly.

ACKNOWLEDGEMENTS

The first author gratefully acknowledges the financial support of a Felix Scholarship granted by the Felix Trust through Oxford University.

REFERENCES

BLIEK, A. 1984 Dynamic analysis of single span cables. Ph.D. thesis, MIT, Cambridge, MA, U.S.A.

BROWN, D. T., LYONS, G. J. & LIN, H. M. 1995 Advances in mooring line damping. *Underwater Technology* **21,** 5–11.

GROSENBAUGH, M. A. & MAVRAKOS, S. A. 1995 Design of oceanographic surface moorings for harsh-weather environments. *SNAME Transactions* **103,** 395–423.

HAGEDORN, P. & SCHÄFER, B. 1980 On non-linear free vibrations of an elastic cable. *International Journal of Non-Linear Mechanics* **15,** 333–340.

HOVER, F. S., GROSENBAUGH, M. A. & TRIANTAFYLLOU, M. S. 1994 Calculation of dynamic tension in towed underwater cable. *IEEE Journal of Oceanic Engineering* **19,** 449–457.

HUANG, S. 1994 Dynamic analysis of 3-D marine cables. *Ocean Engineering* **21,** 587–605.

HUSE, E. & MATSUMOTO, K. 1989 Mooring line damping due to first and second order vessel motion. *Offshore Technology Conference*, Paper OTC 6137.

IRVINE, M. 1981 *Cable Structures*. New York: Dover Publications.

KITNEY, N. & BROWN, D. T. 1998 Efficient prediction of mooring line dynamic loading with experimental verification. *Proceedings of International Conference on Offshore Mechanics and Arctic Engineering*, OMAE 98-0402. New York: ASME.

LEIRA, B. T. 1987 Multidimensional stochastic linearisation of drag forces. *Applied Ocean Research* **9,** 151–163.

LEONARD, J. W. & TUAH, H. 1989 Nonlinear deterministic and stochastic response of cable systems with large bodies under hydrodynamic loads. *Engineering Structures* **8,** 94–107.

LIU, Y. G. & BERGDAHL, L. 1997a Influence of current and seabed friction on mooring cable response: comparison between time-domain and frequency-domain analysis. *Engineering Structures* **19,** 945–953.

LIU, Y. G. & BERGDAHL, L. 1997b Frequency-domain dynamic analysis of cables. *Engineering Structures* **19,** 499–506.
MALHOTRA, A. K. & PENZIEN, J. 1970 Nondeterministic analysis of offshore structures. *ASCE Journal of Engineering Mechanics Division* **96,** 985–1003.
NAKAMURA, N., KOTERAYAMA, W. & KYOZUKA, Y. 1991 Slow drift damping due to drag forces acting on mooring lines. *Ocean Engineering* **18,** 283–296.
PAULLING, J. R. 1979 Frequency domain analysis of OTEC CW pipe and platform dynamics. *Offshore Technology Conference*, Paper OTC 7965.
PAZ, M. 1985 *Structural Dynamics.* New Delhi: CBS publishers.
PEYROT, A. H. 1980 Marine cable structures. *ASCE Journal of Structures Division* **12,** 2391–2400.
ROBERTS, J. B. & SPANOS, P. D. 1990 *Random Vibration and Statistical Linearization.* New York: John Wiley.
SARKAR, A. EATOCK TAYLOR, R. 2000 Effects of mooring line drag damping on response statistics of vessels excited by first and second order excitations. *Ocean Engineering* **27,** 667–686.
SARKAR, A. & MANOHAR, C. S. 1996 Dynamic stiffness matrix of a general cable element. *Archive of Applied Mechanics* **66,** 315–325.
SIMPSON, A. 1972 On the oscillatory motions of translating elastic cables. *Journal of Sound and Vibration* **20,** 177–189.
THOMAS, D. O. & HEARN, G. E. 1994 Deepwater mooring line dynamics with emphasis on sea-bed interference effects. *Offshore Technology Conference*, Paper OTC 7488.
TRIANTAFYLLOU, M. S., BLIEK, A. & SHIN, S. 1985 Dynamic analysis as a tool for open-sea mooring system design. *SNAME Transactions* **93,** 303–324.
WEBSTER, W. C. 1995 Mooring induced damping. *Ocean Engineering* **22,** 571–591.
WU, S. C. & TUNG, C. C. 1975 Random response of offshore structures to wave and current forces. *Sea Grant Publication, UNC-SG-75-22*, Dept of Civil Engineering, North Carolina State University, Rayleigh, NC 27650, U.S.A.